



VOC Gas Sensing Via Microelectronics-Based Absorption Spectroscopy at 220–330 GHz

Tim E. Rice¹ · M. Arshad Zahangir Chowdhury¹ · Muhammad Waleed Mansha² · Mona M. Hella² · Ingrid Wilke³ · Matthew A. Oehlschlaeger¹

Received: 21 May 2020 / Accepted: 4 August 2020 / Published online: 24 August 2020
© Springer-Verlag GmbH Germany, part of Springer Nature 2020

Abstract

Gas sensing by THz wave absorption spectroscopy is demonstrated for several volatile organic compounds (VOCs) using a broadband electronics-based THz wave spectrometer. Spectral absorption is characterized in the frequency range from 220 to 330 GHz for seven VOCs and water vapor in a gas cell at room temperature and pressures of 0.5–10 Torr. Amplitude-modulation is applied to the interrogating radiation, and lock-in detection is used to acquire the transmitted frequency-dependent radiation intensity. For methanol, ethanol, n-propanol, formic acid, formaldehyde, acetaldehyde, acetone, and water vapor, measured transition frequencies agree with literature databases, where available. The present work demonstrates the potential for an all-electronic THz gas sensor for conditions where pressure broadening and line blending occur, as would be found in typical industrial, environmental, and biological gas sensing applications.

1 Introduction

Absorption spectroscopy in the terahertz (THz) or submillimeter frequency band, defined as frequencies from 0.1 to 10 THz ($3.33\text{--}333.3\text{ cm}^{-1}$), provides selective non-intrusive identification of polar gas molecules, including many volatile organic compounds (VOCs), through the interrogation of molecular rotations and low-energy internal torsional modes with resonant external electromagnetic fields [1, 2]. While non-intrusive gas sensing is typically carried out in the infrared region [3–5], the THz region offers several advantages, especially for practical field applications in optically harsh environments. Such environments are found in atmospheric,

combustion, and industrial gas sensing [6]. Additionally, in recent years there have been significant advances in micro, and nano electronic THz frequency devices, enabling a pathway for the development of miniaturized THz wave gas sensors for the detection of a wide array of molecules in a variety of applications [7].

The gas-phase detection of VOCs is of interest in several important industrial and environmental applications. VOCs are unwanted and often controlled hazardous air pollutant emissions [8], resulting from the combustion of fuels, including fossil fuels, biomass, and liquid biofuels. Some VOCs, for example, methanol and ethanol, are also used as combustion fuels, resulting in direct emission to the atmosphere by evaporation or incomplete combustion. Once in the atmosphere, VOCs participate in reactions with nitric oxides and ozone that contribute to photochemical smog [9]. VOCs are involved in a number of chemical and manufacturing processes [10], where they are used as solvents, additives, and/or feedstocks for chemical synthesis; e.g., in the manufacture of plastics, acrylics, rubbers, paints, and pharmaceuticals. VOCs are also used as food preservatives, material sterilizers, and crop pesticides and can be important metabolic markers for biological activity; for example, acetone is a biomarker for diabetes ketoacidosis [11]. Hence, the detection of gaseous VOCs is of interest in a number of diverse applications, in which VOCs may be unwantedly

Electronic supplementary material The online version of this article (<https://doi.org/10.1007/s00340-020-07501-9>) contains supplementary material, which is available to authorized users.

✉ Tim E. Rice
ricet4@rpi.edu

¹ Department of Mechanical, Aerospace, and Nuclear Engineering, Rensselaer Polytechnic Institute, Troy, NY, USA

² Department of Electrical, Computer, and Systems Engineering, Rensselaer Polytechnic Institute, Troy, NY, USA

³ Department of Physics, Applied Physics, and Astronomy, Rensselaer Polytechnic Institute, Troy, NY, USA

released to the atmosphere or where quantitative detection is of importance in engineered or natural processes.

In gas sensing applications, such as those described above, the use of THz frequencies has many optical and spectral advantages over infrared and higher frequencies. Compared to the infrared region, THz waves experience orders-of-magnitude less scattering from particles or aerosols [12]. THz absorption is also effectively immune to particle or aerosol scattering and extinction that so often hinders infrared absorption gas sensors in environments containing aerosols. Interference by water vapor absorption is also reduced in the THz region compared to the infrared region, especially for frequencies less than 1 THz, due to the sparsity of water's rotational absorption lines in this frequency band [13]. Finally, for many polar gas molecules of interest, such as VOCs, THz wave sensing offers strong absorption bands, providing greater sensitivity and/or selectivity than infrared transitions [14].

Prior to recent developments in THz microelectronic sources and detectors, THz absorption studies have mostly been carried out in laboratory settings using large and expensive spectrometers, most notably using frequency-multiplier klystron microwave sources, the FASST Submillimeter Spectroscopy Technique (FASST), and THz time-domain spectroscopy (THz-TDS) methods. FASST provides highly-resolved (kHz) spectroscopy measurements in the 0.1–1 THz frequency range [15–17], where radiation is provided by quasi-optical sources, such as backward wave oscillators, and detection often by high-sensitivity and low time-response Golay cell detectors. FASST methods have been applied for several decades in fundamental spectroscopy studies at extremely low pressure (mTorr) to catalog line positions and strengths, discover and assign transitions, and validate quantum mechanical calculations of rotational energy levels.

THz-TDS methods have been applied to broadband (e.g., 0.1–2 THz) studies at higher pressures, however, with lower resolution (~1 GHz) [12, 14, 18]. THz-TDS measurements have proven to be extremely powerful for selective and sensitive detection (ppm to ppb) of polar compounds, such as VOCs, in the gas phase [14]; however, they are expensive, complex, and not easily applied outside of the laboratory setting.

The last decade has seen major investments in standard silicon-based technologies to increase the cutoff frequencies of active devices (transistors) and enable their operation in the THz regime. Sub-THz wave generation and detection based on such low-cost and high-yield silicon technologies have been reported in complementary metal-oxide semiconductor (CMOS) [7, 19, 20] and silicon germanium (SiGe) [21–23] technologies. As an example, Neese et al. [24] have reported a compact electronic spectrometer operating in the 210–320 GHz frequency range offering detection of

14 gases: acetonitrile, methyl fluoride, acrylonitrile, sulfur dioxide, methyl iodide, methyl bromide, trifluoromethane, acrolein, propionitrile, 1,1 difluoroethene, vinyl fluoride, oxetane, vinyl bromide, and 1,2 dichloroethane. Further examples of microelectronics-based absorption spectroscopy, include the work of Wang and Han [19], which showed gas-phase detection of acetonitrile in the 220–320 GHz frequency range. Hindle et al. [25] developed an electronic absorption sensor for H₂S detection at 611 GHz, while a general-purpose THz wave gas sensors in the 220–270 GHz range [23, 36–28] with application to detection of VOCs have been reported by Schmalz et al. Recently our group has reported on the detection of alcohols using an electronic THz source at high pressures (≥ 5 Torr) [29]. The present study expands on this work by including the characterization of additional VOCs of interest at additional pressures and increasing the resolution and scan rate. The measurements conducted in this report further demonstrate the viability of a high-bandwidth microelectronics-based spectrometer in the 220–330 GHz frequency range for VOC gas sensing, suited for industrial, biological, or environmental applications. Spectral absorption is characterized for pure methanol, ethanol, n-propanol, formic acid, formaldehyde, acetaldehyde, acetone, and water vapor at room temperature and pressures from 0.5 to 10 Torr, conditions where pressure-broadening and transition blending complicate the spectra.

2 Experimental methods

Scanned-frequency absorption spectroscopy measurements were carried out using the hardware implemented in Tekawade et al. [29], including an electronics THz wave source generating radiation from 220 to 330 GHz, a gas cell, and a broadband Schottky diode detector. Experimental procedures and data acquisition methods have been further optimized and improved since the Tekawade et al. study. See Fig. 1 for a photo of the experimental hardware.

Radiation was produced with a Virginia Diodes (VDi) signal generator extension (SGX) module based on planar GaAs Schottky diode technology (model WR 3.4 220–330 GHz), which provided 18-fold frequency multiplication of a radio frequency (RF) input signal. An RF synthesizer (HP model 83752A, 10 MHz–20 GHz) provided the input signal to the SGX module, for the current study at 12.22–18.33 GHz. The high-frequency signal generated by the SGX was directly coupled into a diagonal horn antenna (VDi model WR-3.4) providing free-space radiation propagating away from the horn tip with a 10-degree half-angle (50% power in radiation cone). The diverging beam was collimated with a plano-convex Teflon lens, then passed through the gas cell with two high-density polyethylene (HDPE) windows, and refocused

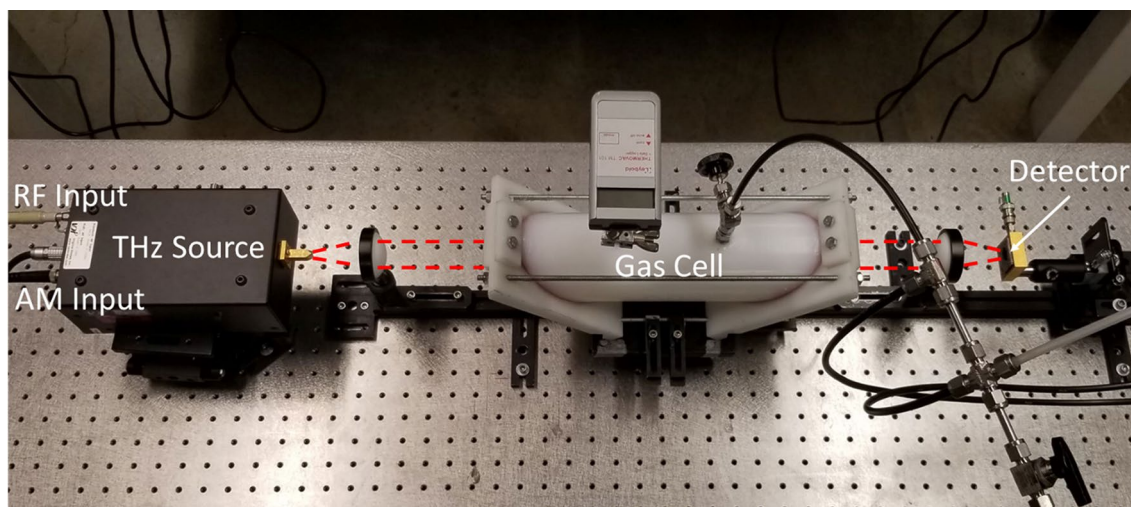


Fig. 1 Experimental setup for scanned-frequency absorption spectroscopy at 220–330 GHz

using a second plano-convex Teflon lens onto a Schottky diode detector (VDi model QOD 3–15).

To increase the signal-to-noise ratio of the measured absorption, amplitude modulation was implemented with lock-in detection. The continuous 220–330 GHz output signal from the SGX module with an output power that ranges from 1 mW at 220 GHz to 0.3 mW at 330 GHz, is digitally chopped at a prescribed modulation frequency using a Keysight 33220A 20 MHz Function/Arbitrary Waveform Generator. The modulation “chopping” signal was sent to the TTL modulation port on the SXG module, producing a square-like output waveform for the 220–330 GHz signal. A modulation frequency of 2.7 kHz was found to yield the greatest degree of noise reduction and most repeatable output intensity–frequency functionality from the SGX module. Higher modulation frequencies led to temporal distortions and instability in the lock-in amplifier out, originating from the limited responsivity of the TTL modulation feature in the SGX module. Lower modulation frequencies require longer lock-in integration times and provide slower frequency sweep rates or data acquisition rates. To improve the frequency sweep rate of the current system, one would need a frequency-multiplier source that can operate at higher modulation frequencies, allowing the use of a shorter lock-in integration time.

The lock-in amplifier (Stanford Research model SR510) was operated in the standard manner, whereby the modulated 220–330 GHz signal was multiplied with a reference single at the same modulated frequency and a reference single at the modulation frequency and shifted in phase by 90° to create two mixed signals. The two mixed signals are then low-pass filtered, with an integration time of 1 ms, to reject noise and harmonic signals and then converted, via a Cartesian-to-polar transformation, to yield a DC amplitude

and phase. The DC amplitude output from the lock-in amplifier is the 220–330 GHz signal intensity used to determine the absorbance of the gas sample of interest.

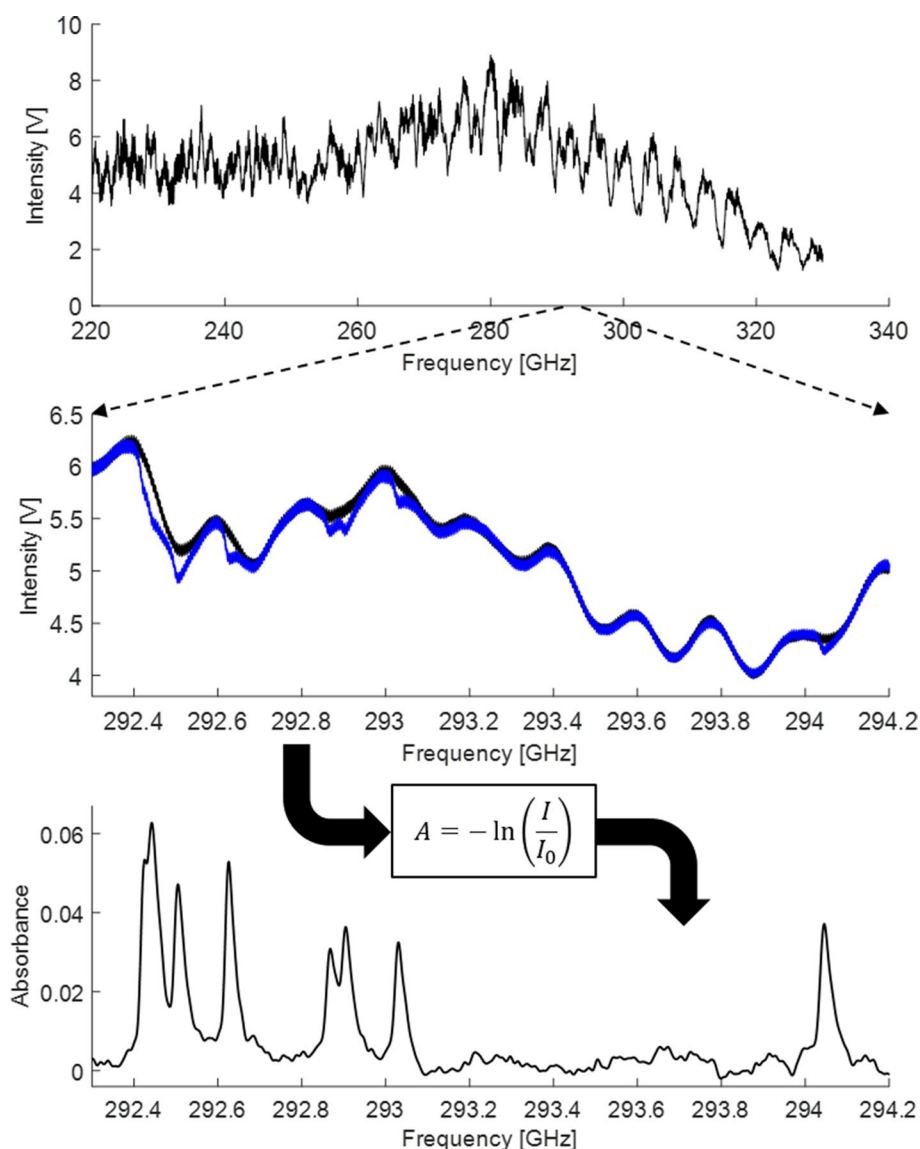
A LabView script was developed and used to trigger the experiment, define and control frequency sweep and amplitude modulation parameters, and acquire and store data. Once triggered, the RF synthesizer frequency sweeps, via a linear ramp function, from 12.22 to 18.33 GHz and the time-dependent 220–330 GHz signal output from the lock-in amplifier, the ramp voltage itself, and data indices were acquired and stored in a.xlsx file. The ramp voltage and data indices are easily converted to the time-dependent radiation frequency.

To determine the spectral absorbance of a gas sample, we measured the reference spectral intensity with the gas cell under vacuum and then filled the gas cell with the gas of interest and repeated the spectral scan, measuring the transmitted signal intensity. Again, both measurements were carried out using the Schottky diode detector and performed using the amplitude modulation methods described above to record the DC frequency-dependent signal intensity. Example reference and signal measurements are shown in Fig. 2. The absorbance of the gas sample can be described using the Beer-Lambert law:

$$A = \epsilon cl = -\ln(I/I_0),$$

where the absorption coefficient, $\epsilon = \epsilon(T, c, f)$, is a function of temperature (T), molar concentrations (c) (through pressure broadening), and frequency (f). The absorbance, A , scales linearly with the optical path length, $l = 21.59$ cm (in present experiments), and the absorbers concentration, c . The absorption coefficient (ϵ) contains information about the line shape for each transition and is also a function of the

Fig. 2 Example experiment carried out for pure formic acid (HCOOH) at 1 Torr and 297 K. Top graph: reference intensity (I_0), middle graph: reference (I_0 , black) and measured (I , blue) intensities; bottom graph: absorbance (A)



concentrations of constituents present in the absorbing gas, through their influence on line shape via collisional or pressure broadening. Again, the reference and measured signal intensities, I_0 and I , are measured under vacuum and with the absorbing gas of interest in the gas cell, respectively. Finally, the absorbance is passed through a low-pass filter to reduce any high-frequency noise, mostly emanating from the detector. See Fig. 2 for an example absorbance measurement of formic acid (HCOOH). In the Fig. 2 example, the frequency was swept at 4.7 GHz/s from 220 to 330 GHz, the lock-in amplifier operated at an integration time of 1 ms, and a cutoff filter of 300 Hz is used to increase the signal-to-noise of the absorbance signal. The final spectral resolution under these operating parameters is 15 MHz, where the spectral features of interest have half-widths of ≥ 50 MHz, and the noise floor or detection limit is ± 0.001 to ± 0.003 in

absorbance. The noise is composed of high-frequency content originating from the electronics that make up the source and detector, and low-frequency noise resulting from standing waves that subtly fluctuate due to optical path variation (caused by the index of refraction differences, slight bending of cell walls due to pressure/vacuum, and human error), such that they cannot wholly be canceled using common-mode noise rejection (e.g., division of absorbed and reference signal in the Beer-Lambert law). Improvements to the sensor could be made by reducing the electronics noise, increasing the THz power, and refining the optical configuration.

Table 1 Compounds and pressures for which spectral absorption measurements were carried out. All experiments performed at 297 K and for 220–330 GHz

Compound	Molecular formula	Pressures [Torr]
Methanol	CH ₃ OH	1, 2, 4, 8
Ethanol	CH ₃ CH ₂ OH	1, 2, 4
n-Propanol	CH ₃ CH ₂ CH ₂ OH	2, 4, 8
Formic acid	HCOOH	0.5, 1, 2, 4, 8
Formaldehyde/ water vapor/ methanol	H ₂ CO / H ₂ O / CH ₃ OH	0.5, 1, 2 (total pressure)
Acetaldehyde	CH ₃ CHO	0.5, 1, 2
Acetone	CH ₃ COCH ₃	0.5, 1, 2, 4, 8
Water vapor	H ₂ O	10

3 Results

Spectral absorption in the 220–330 GHz frequency range was characterized at 297 K for a range of VOCs listed in Table 1. All experiments were performed using pure reagent-grade chemicals, with the exception of formaldehyde, which was vaporized from a formaldehyde/water/methanol solution. The experimental results have been appended in the electronic supplementary material. The compounds studied were chosen due to their appreciable absorption in the accessible frequency range and their importance in industrial applications (e.g., energy, combustion, and manufacturing), biological systems, medical diagnoses, and/or as atmospheric pollutants. The gases studied include alcohols, ketones, aldehydes, carboxylic acids, and water vapor.

Although there is substantial prior fundamental experimental work on the rotational spectroscopy of small VOCs carried out at very low pressures (~mTorr) where features

Fig. 3 Absorption measurements for pure methanol at 2 Torr (black line), with comparison to HITRAN-based [41] spectral simulations (blue dashed line). The path length is 21.59 cm

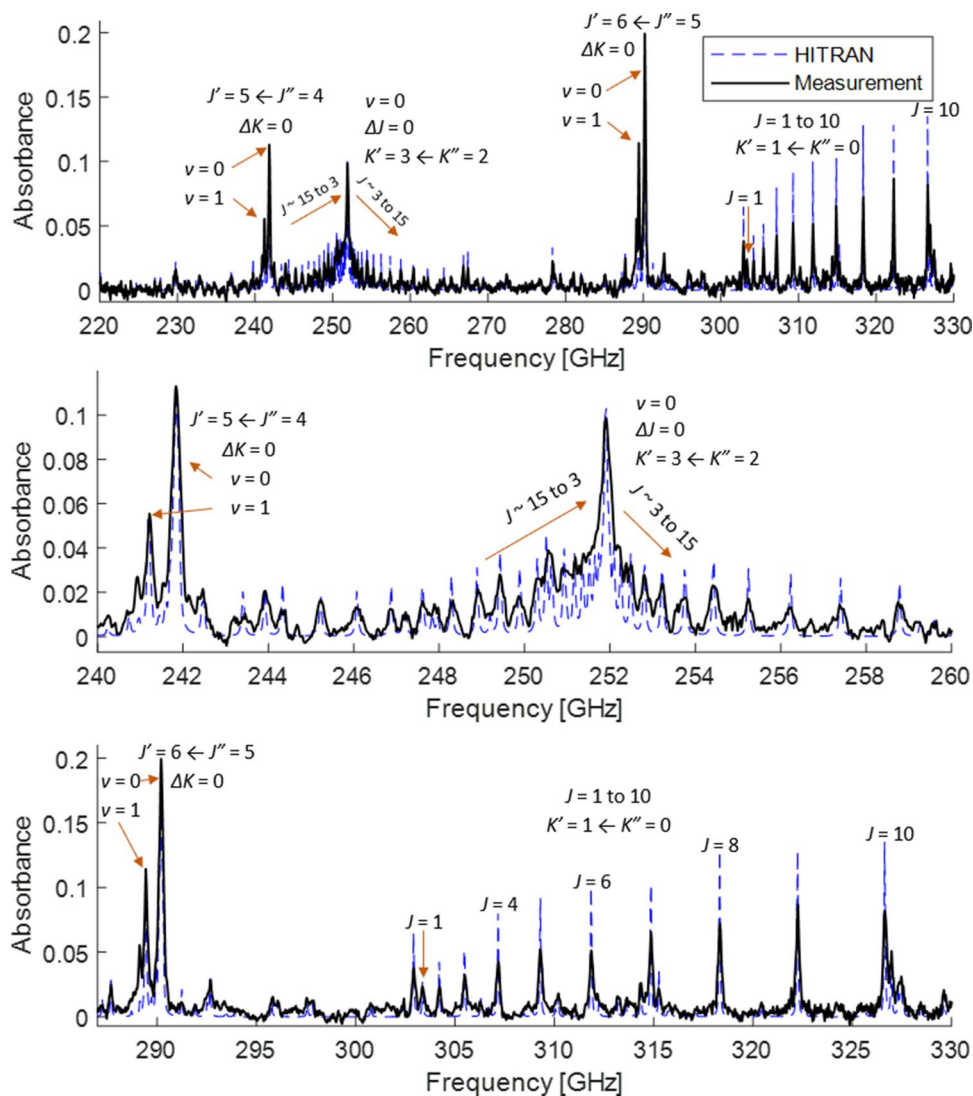
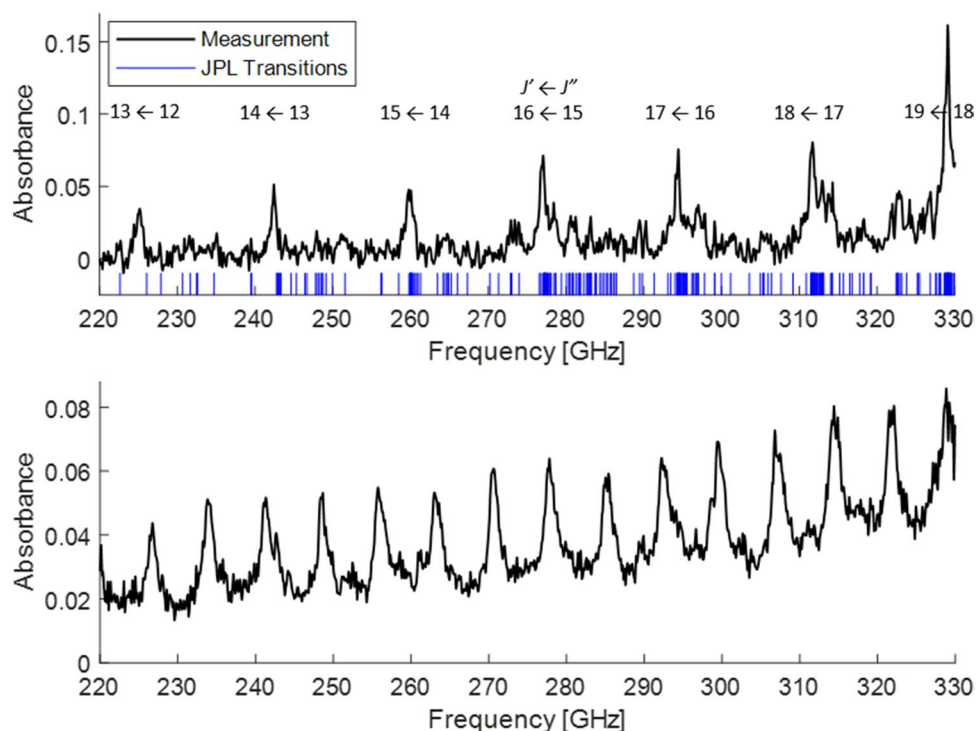


Fig. 4 Absorption measurements for pure ethanol at 4 Torr (top) and pure n-propanol at 8 Torr (bottom). Transitions for ethanol are from the JPL molecular spectroscopy database [40]



are well separated and in the Doppler limit, there is limited study of the absorption of these compounds under appreciable pressures and using microelectronics-based sub-THz sources suitable for the development of commercial gas sensors [26, 33–39, 42–54].

3.1 Alcohols

Measurements for the three alcohols characterized are shown in Figs. 3 and 4. In the case of methanol (Fig. 3), an asymmetric top molecule, the features observed in the 220–330 GHz range are rotational transitions that occur in both the ground and the first vibrationally-excited state. The features are labeled in Fig. 3 according to vibrational quantum number (ν), the quantum number for total rotational angular momentum (J), and the quantum number for the projection of J onto the a -inertial axis (K). For methanol, the a -axis is parallel to the methyl top axis. The J'' and J' and K'' and K' symbols represented the quantum numbers for the lower and upper states, respectively. The strong features in the frequency range of interest include transitions for $J' = 5 \leftarrow J'' = 4$ and $\Delta K = 0$ at 241 GHz and $J' = 6 \leftarrow J'' = 5$ and $\Delta K = 0$ at 290 GHz. These features are split into a primary peak for transitions in the ground vibrational state and a secondary peak, shifted to lower frequencies, resulting from rotational transitions in the first excited vibrational state. The other strong methanol features in this frequency range include a blended feature at 252 GHz for $\Delta J = 0$ and $K' = 3 \leftarrow K'' = 2$ and a series of features from 302

to 328 GHz for $J = 1$ to 10 ($\Delta J = 0$) and $K' = 1 \leftarrow K'' = 0$. The present measurements are in good agreement with the HITRAN simulations for line locations and reasonable agreement of integrated absorbance; however, the present study shows a bit more collisional line broadening than predicted by the HITRAN database. Collisional line broadening parameters could be a topic worthy of future experimental study.

For ethanol and n-propanol (Fig. 4), we observe repeating and blended spectral features, due to the pressure broadening of the multitude of closely spaced transitions. Ethanol is a near-prolate asymmetric top (i.e., $A > B \approx C$) with rotational constants: $A = 34.9$, $B = 9.35$ and $C = 8.14$ GHz [36]. Near-prolate asymmetric tops often exhibit strong repeating R -branch a -type transitions (i.e., $\Delta J = +1$, $\Delta K_a = 0$, and $\Delta K_c = +1$) centered at frequencies of $(B + C)(J'' + 1)$ and spaced at frequency intervals of $(B + C)$. For an asymmetric top molecule, J is the quantum number for total rotational angular momentum and K_a and K_c are the quantum labels for the projection of total angular momentum onto the a - and c -axes, respectively.

Like ethanol, n-propanol is also a near-prolate asymmetric top, but with five stable conformers it has very complex rotational spectroscopy [37]. The present measurements for n-propanol (Fig. 4 bottom panel) show strong blended features that repeat approximately every 7 GHz. The observed spectral features, repeating every ~ 7 GHz, are due to R -branch a -type transitions of the T_t and T_g conformers. Rotational constants for these two conformers are: $A = 26.6$,

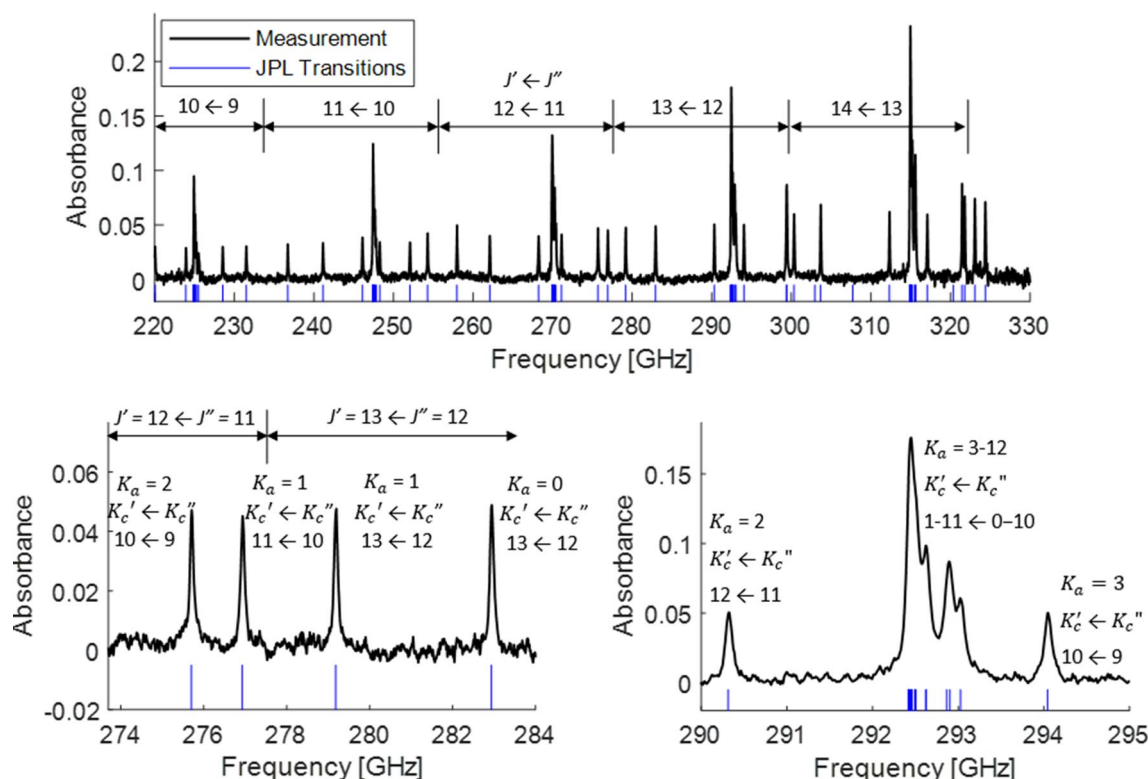


Fig. 5 Absorption measurements for pure formic acid at 4 Torr. Labeled transitions and frequencies are from the JPL molecular spectroscopy database [40]

$B = 3.8$, and $C = 3.5$ GHz for the Tt conformer and $A = 26.1$, $B = 3.7$, and $C = 3.5$ GHz for the Tg conformer [37]. The rotational constants result in strong R -branch a -type transitions spaced at $(B + C) = 7.2 - 7.3$ GHz, as observed experimentally in the repeating broad n -propanol absorption features (Fig. 4 bottom panel).

3.2 Formic acid

The measured absorption spectra for formic acid in the 220–330 GHz range is shown in Fig. 5. Like ethanol and n -propanol, formic acid is a near-prolate asymmetric top. However, for formic acid, we observe distinct transitions, rather than blended transitions as in ethanol and n -propanol. Formic acid has rotational constants of $A = 77.51$, $B = 12.06$, and $C = 10.42$ GHz [44], resulting in spacing for R -branch a -type transitions ($\Delta J = +1$, $\Delta K_a = 0$, and $\Delta K_c = +1$) of $(B + C) = 22.4$ GHz, with transitions centered at $(B + C)(J'' + 1)$ for $J'' = 9 - 13$ in the 220–330 GHz frequency range [40, 41]. In the present frequency range, R -branch b -type transitions also exist, with $\Delta J = +1$ and a simultaneous change in K_a and K_c ; however, these transitions are too weak to be experimentally observed against the noise floor. The formic acid transitions are shown in Fig. 5 are spaced every 22.4 GHz and grouped by $J' \leftarrow J''$, with each

transition occurring for a specific K_a and $K_c' \leftarrow K_c''$. For large values of K_a , the transitions converge and blended spectral features are observed at 225.1, 247.6, 270.1, 292.6, and 315.2 GHz.

3.3 Aldehydes

Figure 6 illustrates measured absorption spectra for formaldehyde, where formaldehyde was prepared in the gas phase from the evaporation of a formaldehyde/water/ethanol solution at 37 mass-% formaldehyde (i.e., formalin). The resulting gaseous mixture, for which spectral absorption was characterized, was primarily water vapor (~ 90 – 95%) with 2–3% formaldehyde. In Fig. 6 strong and narrow R -branch a -type transitions are observed for formaldehyde, similar to formic acid. Rotational constants for formaldehyde, a near-prolate asymmetric top, are $A = 281.97$, $B = 38.8$, and $C = 34.0$ GHz [45].

Spectral absorption measurements for acetaldehyde are shown in Fig. 7. Acetaldehyde is another near-prolate asymmetric top, with rotational constants of $A = 56.49$, $B = 10.45$, and $C = 9.09$ GHz [46]. The acetaldehyde spectrum is significantly more complex than that for formaldehyde, containing many more transitions, some of which overlap. Again, strong R -branch a -type transitions are mostly observed with

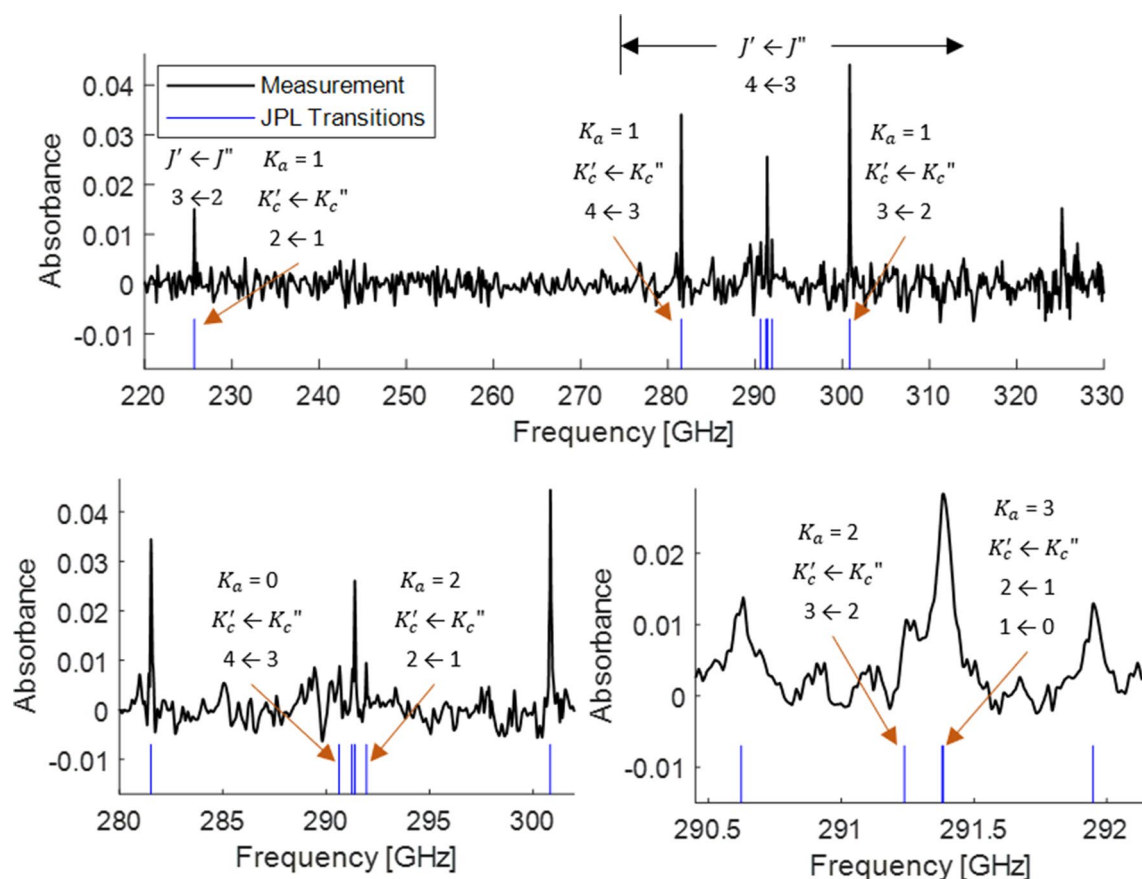


Fig. 6 Absorption measurements for gaseous formaldehyde/water vapor/methanol at a total pressure of 2 Torr and containing approximately 2–3% formaldehyde. Labeled transitions and frequencies are

from the JPL molecular spectroscopy database [40]. The bottom two graphs are for $J' = 4 \leftarrow J'' = 3$

strong and significantly blended spectral features, spaced at $(B + C)$ with a few weak R -branch b -type also observable in the spectral range.

3.4 Acetone

Spectral absorption measurements made for acetone are shown in Fig. 8 and illustrate discrete spectral features that sit on top of a broad continuum absorption that increases in strength with increasing frequency. The continuum absorption has been observed in prior studies using THz-TDS and Fourier transform spectrometer methods to interrogate broadband acetone absorption in the THz frequency range [55,56, 57]. In the present study, the continuum acetone absorption is observed to increase with the square of the pressure and, therefore, we presume occurs for similar reasons as to the well-studied absorption continuum for water vapor in the far infrared and into the microwave region. For water vapor, the mechanisms responsible for its rotational continuum include absorption in the intermediate to far wings of transitions, that is not accounted for in

conventional line shape models, and absorption that occurs due to metastable dimers that result from biomolecular collisional events.

Acetone is a quasi-oblate asymmetric top ($A \approx B > C$) with rotational constants of $A = 10.17$, $B = 8.52$, and $C = 4.91$ GHz [54]. The discrete and repeatedly spaced acetone transitions observed in the current frequency range are spaced at $2C$, corresponding to R -branch b -type transitions. The frequencies of the discrete and numerous acetone transitions are in good agreement with literature values [40, 54] from a combination of high-resolution experiments and theory, and can be assigned to both R -branch b -type and a -type transitions.

3.5 Water vapor

Absorption by pure water vapor was characterized to verify potential interference from this ubiquitous atmospheric gas on VOC gas sensing in the present frequency range. See Fig. 9 for an absorption measurement for water vapor at 10 Torr which illustrates that water vapor absorption in the

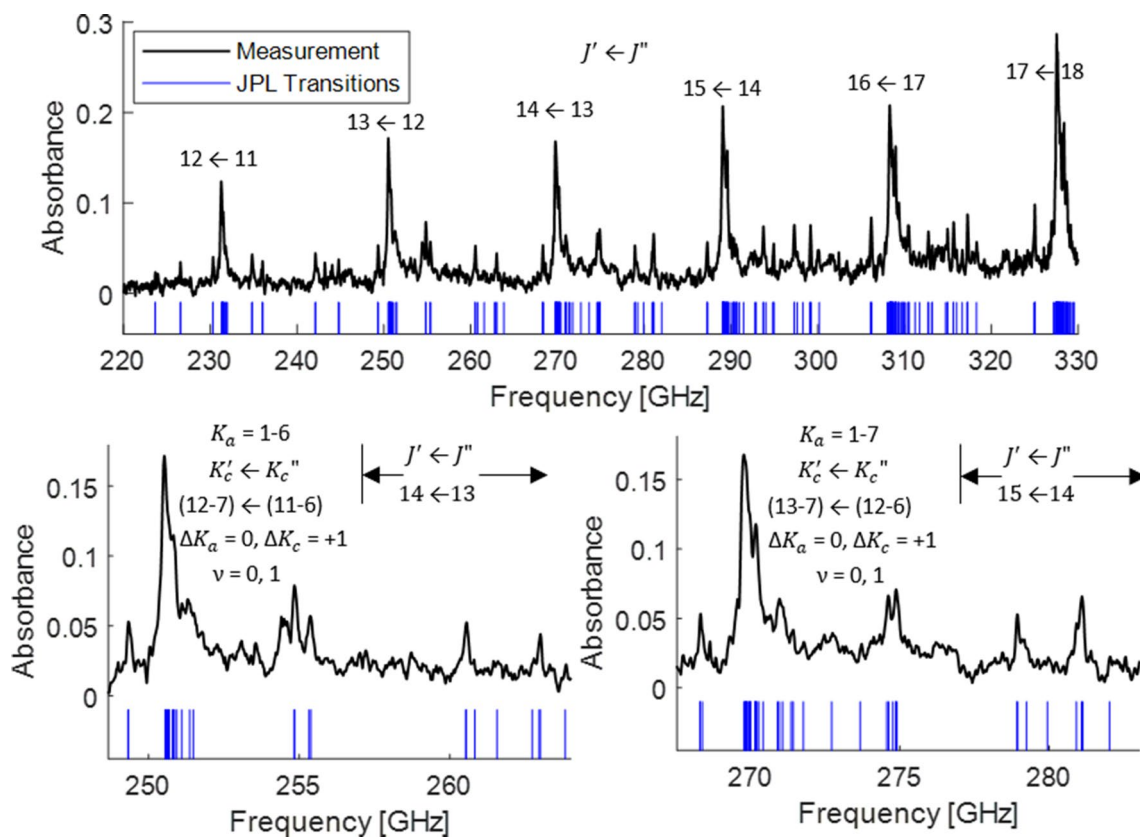


Fig. 7 Absorption measurements for pure acetaldehyde at 1 Torr. Labeled transitions and frequencies are from the JPL molecular spectroscopy database [40]

investigated frequency range is negligible with the exception of a weak line at 325.15 GHz for the $J' = 5 \leftarrow J'' = 4$, $K_a' = 1 \leftarrow K_a'' = 2$, and $K_c' = 5 \leftarrow K_c'' = 2$ transition.

4 Discussion

Measured absorption in the 220–330 GHz frequency range for the seven VOCs characterized in the present study are compared in Fig. 10. The spectra illustrate several potential frequencies for selective gas sensing of each species in a multi-component mixture, depending on what species are present. For the alcohols, there are many frequency locations for the simultaneous measurement of methanol and ethanol. For a ternary mixture of the three alcohols considered, the broad n-propanol spectrum complicates the identification of isolated spectral features; however, there are features at 250–260 and 285–300 GHz that provide sufficient specificity for the simultaneous detection of the three alcohols. Similarly, formic acid, formaldehyde, acetaldehyde, and acetone have many isolated features, with acetone, the weakest

absorber, the most difficult to detect. For example, in the 300–330 GHz window, several isolated features exist for the detection of these four VOC species.

The present results illustrate the potential for microelectronics-based THz wave gas sensing for VOCs. As illustrated throughout the results section, the spectral measurements are in good agreement with literature databases [40, 41], in terms of line positions. However, in most cases, pressure broadening parameters either are not available or have been assumed for the target VOC species in the present spectral range. Furthermore, few if any previous studies have been carried out at appreciable pressures, such that would be found in many gas sensing applications. Even at the relatively modest pressures encountered in the present study, pressure broadening controls the observed line shapes and many of the seemingly discrete features are, in fact, combinations of many transitions. Both the measurement of pressure broadening parameters and the extension of THz gas sensing capabilities to higher pressures are areas in which future investigations would be welcome. While the present study and recent literature [19–32] show the power of

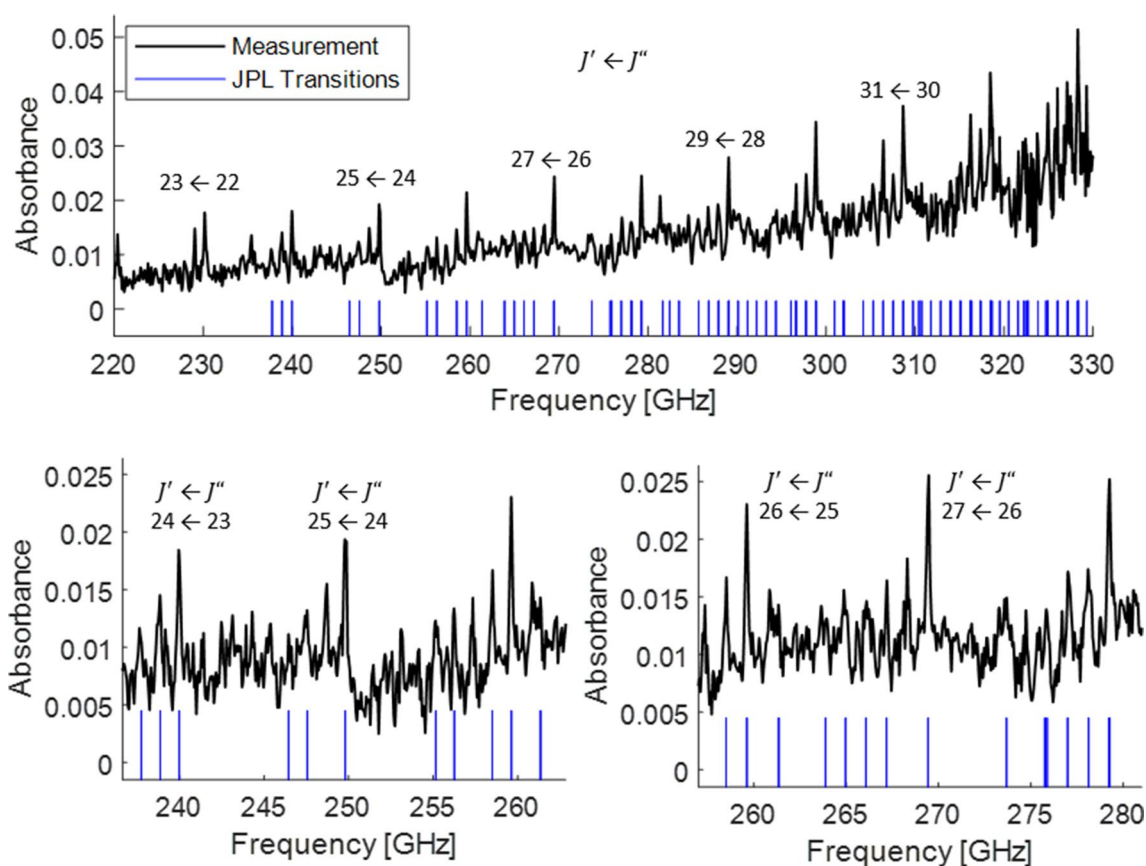
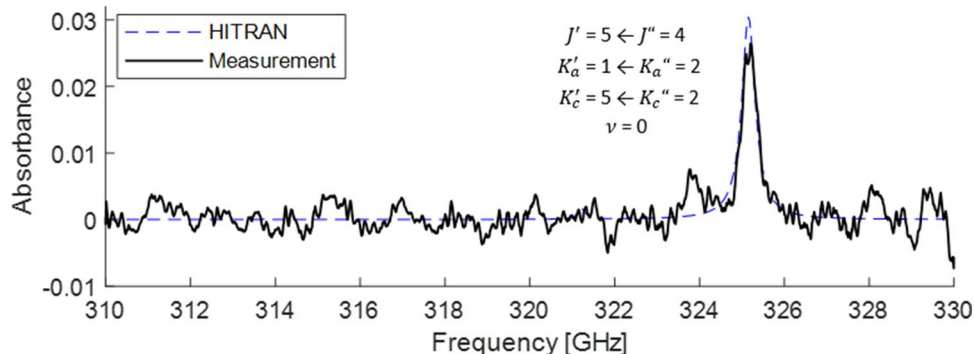


Fig. 8 Absorption measurements for pure acetone at 1 Torr. Labeled transitions and frequencies are from the JPL molecular spectroscopy database [40]

Fig. 9 Absorption measurement for pure water vapor at 10 Torr with comparison to HITRAN-based spectral simulation [41]

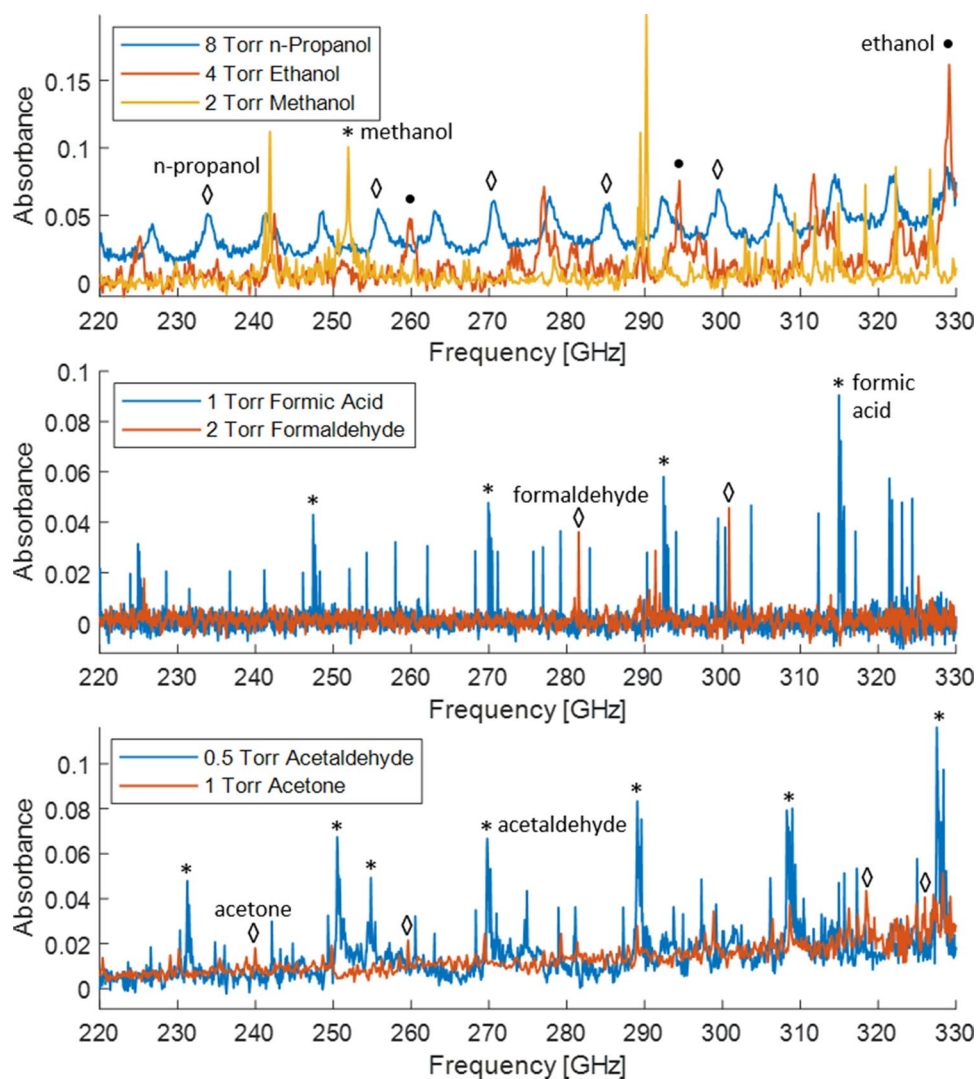


microelectronics-based THz wave systems for selective and sensitive gas sensing, future development of miniaturized and robust THz wave sources and sensors is needed for THz wave gas sensing to become a commercial reality.

5 Summary

Volatile organic compound (VOC) gas sensing using a high-bandwidth microelectronics-based THz wave spectrometer, based on a radio frequency multiplier source and Schottky diode detector, is demonstrated for pure methanol, ethanol, n-propanol, formic acid, formaldehyde, acetaldehyde, and acetone. Spectral absorption measurements

Fig. 10 Comparison of absorption spectra for the seven VOCs characterized in the current study



were made in the 220 – 330 GHz frequency range using an amplitude-modulation method with lock-in detection for the seven VOCs and water vapor at room temperature and pressures of 0.5 – 10 Torr, conditions where pressure-broadening often results in complex blended spectra. Measured spectral absorption and transition frequencies agree well with literature databases. The potential applications for microelectronics THz wave gas sensing for VOCs are significant, including monitoring combustion and other energy systems where VOCs are byproducts, chemical processes and materials synthesis where VOCs are feedstocks and byproducts, biological or medical systems where VOCs result from metabolic processes, and the environment where VOC emissions result from anthropogenic and naturogenic sources.

Acknowledgement This work was supported by the National Science Foundation under Grant CBET-1851291.

References

1. S. Svanberg, *Atomic and Molecular Spectroscopy: Basic Aspects and Practical Applications* (Springer Science & Business Media, Berlin, 2012)
2. H.H. Mantsch, D. Naumann, *J. Mol. Struct.* **964**, 1 (2010)
3. P. Werle, F. Slemr, K. Maurer, R. Kormann, R. Mücke, B. Jänker, *Opt. Lasers Eng.* **37**, 101 (2002)
4. A.A. Kosterev, F.K. Tittel, *IEEE J. Quantum Electron.* **38**, 582 (2002)
5. C. S. Goldenstein, R. Mitchell Spearrin, J. B. Jeffries, and R. K. Hanson, *Progress Energy Comb. Sci.* **60**, 132 (2017)
6. M. Naftaly, N. Vieweg, and A. Deninger, *Sensors* **19**, (2019)
7. M. W. Mansha, K. Wu, T. E. Rice, M. A. Oehlschlaeger, M. M. Hella, and I. Wilke, *IEEE. Sensors* (2019)
8. R. Friedrich and A. Obermeier, *Reactive Hydrocarbons in the Atmosphere 1* (1999)
9. R. G. Derwent, *Issues in Environmental Science and Technology 1* (n.d.)
10. B.C. McDonald, J.A. de Gouw, J.B. Gilman, S.H. Jathar, A. Akherati, C.D. Cappa, J.L. Jimenez, J. Lee-Taylor, P.L. Hayes, S.A. McKeen, Y.Y. Cui, S.-W. Kim, D.R. Gentner, G.

- Isaacman-VanWertz, A.H. Goldstein, R.A. Harley, G.J. Frost, J.M. Roberts, T.B. Ryerson, M. Trainer, *Science* **359**, 760 (2018)
11. T.P.J. Blaikie, J.A. Edge, G. Hancock, D. Lunn, C. Megson, R. Peverall, G. Richmond, G.A.D. Ritchie, D. Taylor, *J. Breath Res.* **8**, 046010 (2014)
 12. Y.-D. Hsieh, S. Nakamura, D.G. Abdelsalam, T. Minamikawa, Y. Mizutani, H. Yamamoto, T. Iwata, F. Hindle, T. Yasui, *Sci. Rep.* **6**, 28114 (2016)
 13. M. Exter, C. Fattinger, D. Grischkowsky, *Opt. Lett.* **14**, 1128 (1989)
 14. R.M. Smith, M.A. Arnold, *Anal. Chem.* **87**, 10679 (2015)
 15. D.T. Petkie, T.M. Goyette, R.P.A. Bettens, S.P. Belov, S. Albert, P. Helminger, F.C. De Lucia, *Rev. Sci. Instrum.* **68**, 1675 (1997)
 16. S. Albert, D.T. Petkie, R.P. Bettens, S.P. Belov, F.C. De Lucia, *Anal. Chem.* **70**, 719A (1998)
 17. F. C. De Lucia and D. T. Petkie, *Terahertz for Military and Security Applications III* (2005)
 18. P. Kilcullen, I.D. Hartley, E.T. Jensen, M. Reid, *J. Infrared Millimeter Terahertz Waves* **36**, 380 (2015)
 19. C. Wang, R. Han, *IEEE J. Solid-State Circuits* **52**, 3361 (2017)
 20. R. Han, Z. Hu, C. Wang, J. Holloway, X. Yi, M. Kim, J. Mawdsley, *IEEE Microwave Mag.* **20**, 80 (2019)
 21. P. Chevalier, T. F. Meister, B. Heinemann, S. Van Huylenbroeck, W. Liebl, A. Fox, A. Sibaja-Hernandez, and A. Chantre, 2011 IEEE Bipolar/BiCMOS Circuits and Technology Meeting (2011)
 22. D. Wang, K. Schmalz, M.H. Eissa, J. Borngraber, M. Kucharski, M. Elkhoully, M. Ko, H.J. Ng, D. Kissinger, *IEEE Trans. Microw. Theory Tech.* **66**, 4232 (2018)
 23. K. Schmalz, N. Rothbart, M.H. Eissa, J. Borngraber, D. Kissinger, H.-W. Hübers, *AIP Adv.* **9**, 015213 (2019)
 24. C.F. Neese, I.R. Medvedev, G.M. Plummer, A.J. Frank, C.D. Ball, F.C. De Lucia, *IEEE Sens. J.* **12**, 2565 (2012)
 25. F. Hindle, L. Kuuliala, M. Mouelhi, A. Cuisset, C. Bray, M. Vanwolleghem, F. Devlieghere, G. Mouret, R. Bocquet, *Analyst* **143**, 5536 (2018)
 26. K. Schmalz, J. Borngraber, W. Debski, M. Elkhoully, R. Wang, P.F.-X. Neumaier, D. Kissinger, H.-W. Hubers, *IEEE Trans. Terahertz Sci. Technol.* **6**, 318 (2016)
 27. K. Schmalz, N. Rothbart, P.F.-X. Neumaier, J. Borngraber, H.-W. Hubers, D. Kissinger, *IEEE Trans. Microw. Theory Tech.* **65**, 1807 (2017)
 28. N. Rothbart, K. Schmalz, and H.-W. Hubers, 2019 44th International Conference on Infrared, Millimeter, and Terahertz Waves (IRMMW-THz) (2019)
 29. A. Tekawade, T. E. Rice, M. A. Oehlschlaeger, M. W. Mansha, K. Wu, M. M. Hella, and I. Wilke, *Appl. Phys. B* **124**, (2018)
 30. R. Han, E. Afshari, *IEEE J. Solid-State Circuits* **48**, 3090 (2013)
 31. K. Wu, S. Muralidharan, M.M. Hella, *IEEE Trans. Electron Devices* **65**, 788 (2018)
 32. L. Yang, T. Guo, X. Zhang, S. Cao, and X. Ding, *Rev. Analyt. Chem.* **37**, (2018)
 33. R.M. Lees, F.J. Lovas, W.H. Kirchhoff, D.R. Johnson, *J. Phys. Chem. Ref. Data* **2**, 205 (1973)
 34. F.C. De Lucia, E. Herbst, T. Anderson, P. Helminger, *J. Mol. Spectrosc.* **134**, 395 (1989)
 35. L.-H. Xu, F.J. Lovas, *J. Phys. Chem. Ref. Data* **26**, 17 (1997)
 36. F.J. Lovas, *J. Phys. Chem. Ref. Data* **11**, 251 (1982)
 37. Z. Kisiel, O. Dorosh, A. Maeda, I.R. Medvedev, F.C. De Lucia, E. Herbst, B.J. Drouin, J.C. Pearson, S.T. Shipman, *Phys. Chem. Chem. Phys.* **12**, 8329 (2010)
 38. I. R. Medvedev, R. Schueler, J. Thomas, O. Kenneth, H.-J. Nam, N. Sharma, Q. Zhong, D. J. Lary, and P. Raskin, 2016 41st International Conference on Infrared, Millimeter, and Terahertz Waves (IRMMW-THz) (2016)
 39. A.M. Fosnight, B.L. Moran, I.R. Medvedev, *Appl. Phys. Lett.* **103**, 133703 (2013)
 40. H.M. Pickett, R.L. Poynter, E.A. Cohen, M.L. Delitsky, J.C. Pearson, H.S.P. Müller, *J. Quant. Spectrosc. Radiat. Transfer* **60**, 883 (1998)
 41. I.E. Gordon, L.S. Rothman, C. Hill, R.V. Kochanov, Y. Tan, P.F. Bernath, M. Birk, V. Boudon, A. Campargue, K.V. Chance, B.J. Drouin, J.M. Flaud, R.R. Gamache, J.T. Hodges, D. Jacquemart, V.I. Perevalov, A. Perrin, K.P. Shine, M.A.H. Smith, J. Tennyson, G.C. Toon, H. Tran, V.G. Tyuterev, A. Barbe, A.G. Császár, V.M. Devi, T. Furtenbacher, J.J. Harrison, J.M. Hartmann, A. Jolly, T.J. Johnson, T. Karman, I. Kleiner, A.A. Kyuberis, J. Loos, O.M. Lyulin, S.T. Massie, S.N. Mikhailenko, N. Moazzen-Ahmadi, H.S.P. Müller, O.V. Naumenko, A.V. Nikitin, O.L. Polyansky, M. Rey, M. Rotger, S.W. Sharpe, K. Sung, E. Starikova, S.A. Tashkun, J.V. Auwera, G. Wagner, J. Wilzewski, P. Wcisło, S. Yu, E.J. Zak, *J. Quant. Spectrosc. Radiat. Transf.* **203**, 3 (2017)
 42. M. Winnewisser, B.P. Winnewisser, M. Stein, M. Birk, G. Wagner, G. Winnewisser, K.M.T. Yamada, S.P. Belov, O.I. Baskakov, *J. Mol. Spectrosc.* **216**, 259 (2002)
 43. O.I. Baskakov, B.P. Winnewisser, I.R. Medvedev, F.C. De Lucia, *J. Mol. Struct.* **795**, 42 (2006)
 44. J. V. Auwera and J. Vander Auwera, *J. Molec. Spectrosc.* **155**, 136 (1992)
 45. D.R. Johnson, F.J. Lovas, W.H. Kirchhoff, *J. Phys. Chem. Ref. Data* **1**, 1011 (1972)
 46. I. Kleiner, F.J. Lovas, M. Godefroid, *J. Phys. Chem. Ref. Data* **25**, 1113 (1996)
 47. R. Bocquet, J. Demaison, L. Poteau, M. Liedtke, S. Belov, K.M.T. Yamada, G. Winnewisser, C. Gerke, J. Gripp, T. Köhler, *J. Mol. Spectrosc.* **177**, 154 (1996)
 48. S. Brünken, H.S.P. Müller, F. Lewen, G. Winnewisser, *Phys Chem Chem Phys* **5**, 1515 (2003)
 49. I.A. Smirnov, E.A. Alekseev, V.V. Ilyushin, L. Margulés, R.A. Motiyenko, B.J. Drouin, *J. Mol. Spectrosc.* **295**, 44 (2014)
 50. A. Omar, S. Eliet, A. Cuisset, G. Dhont, C. Coeur-Tourneur, R. Bocquet, G. Mouret, F. Hindle, *IEEE Sens. J.* **15**, 6141 (2015)
 51. N. Rothbart, O. Holz, R. Koczulla, K. Schmalz, and H.-W. Hübers, *Sensors* **19**, (2019)
 52. P.F.-X. Neumaier, K. Schmalz, J. Borngraber, R. Wylde, H.-W. Hübers, *Analyst* **140**, 213 (2015)
 53. J.M. Vacherand, B.P. Van Eijck, J. Burie, J. Demaison, *J. Mol. Spectrosc.* **118**, 355 (1986)
 54. P. Groner, S. Albert, E. Herbst, F. C. De Lucia, F. J. Lovas, B. J. Drouin, and J. C. Pearson, *The Astrophysical Journal Supplement Series* **142**, 145 (2002)
 55. Ilyushin, E. A. Alekseev, O. A. Dorovskaya, R. A. Motiyenko, and L. Margules, 2015 International Young Scientists Forum on Applied Physics (YSF) (2015)
 56. L. Chen, S. Oishi, *Rev. Laser Eng.* **34**, 251 (2006)
 57. R. E. Peale, A. V. Muravjov, J. W. Cleary, T. Brusentsova, C. J. Fredricksen, G. D. Boreman, V. L. Vaks, A. V. Maslovsky, and S. D. Nikifirov, *Optical Terahertz Science and Technology* (2007)

Publisher's Note Springer Nature remains neutral with regard to jurisdictional claims in published maps and institutional affiliations.